High-Content RNAi Phenotypic Screening Unveils the Involvement of Human Ubiquitin-Related Enzymes in Late Cytokinesis

Mikaël Boullé, Laurianne Davignon, Keïs Nabhane Saïd Halidi, Salomé Guez, Emilie Giraud, Marcel Hollenstein, Fabrice Agou

Article

High-Content RNAi Phenotypic Screening Unveils the Involvement of Human Ubiquitin-Related Enzymes in Late Cytokinesis

Mikaël Boullé [1,2,*], Laurianne Davignon [1], Keïs Nabhane Saïd Halidi [1,3], Salomé Guez [1], Emilie Giraud [1], Marcel Hollenstein [2], and Fabrice Agou [1,*]

[1] Institut Pasteur, Université Paris Cité, CNRS UMR 3523, Chemogenomic and Biological Screening Core Facility, Center for Technological Resources and Research (C2RT), Department of Structural Biology and Chemistry, F-75015 Paris, France
[2] Institut Pasteur, Université Paris Cité, CNRS UMR 3523, Laboratory for Bioorganic Chemistry of Nucleic Acids, Department of Structural Biology and Chemistry, F-75015 Paris, France
[3] Sorbonne Université, Collège doctoral, F-75005 Paris, France
* Correspondence: MB, mikael.boulle@pasteur.fr, Tel.: (+33) 1 40 61 39 45; FA, fabrice.agou@pasteur.fr, Tel.: (+33) 1 44 38 95 69

Abstract: CEP55 is a central regulator of late cytokinesis overexpressed in numerous cancers. Its post-translationally controlled recruitment to the midbody is crucial to the structural coordination of the abscission sequence. Our recent evidence that CEP55 contains two Ubiquitin-Binding Domains was the first structural and functional link between Ubiquitin signaling and ESCRT-mediated severing of the intercellular bridge. So far high-content screens focusing on cytokinesis used multinucleation as endpoint readout. Here, we report an automated image-based detection method of intercellular bridges, which we applied to further our understanding of late cytokinetic signaling by performing an RNAi screen of Ubiquitin ligases and deubiquitinases. A secondary validation confirmed four candidate genes, i.e. *LNX2*, *NEURL*, *UCHL1* and *RNF157*, whose downregulation variably affects interconnected phenotypes related to CEP55 and its UBDs: decreased recruitment of CEP55 to the midbody, increased number of midbody remnants per cell, increased frequency of intercellular bridges or multinucleation events. It brings into question the Notch-dependent or independent contributions of LNX2 and NEURL to late cytokinesis. Similarly, the role of UCHL1 in autophagy could link its function with the fate of midbody remnants. Beyond the biological interest, this high-content screening approach could also be used to isolate anticancer drugs that act by impairing cytokinesis and CEP55 functions.

Keywords: cytokinesis; CEP55; Ubiquitin signaling; RNAi; image analysis tool; high-content screening

1. Introduction

The achievement of complete cell division requires both the separation of the nuclear and the cytoplasmic content [1]. However, the comprehension of mitosis is far more advanced than the knowledge about cytokinesis [2,3]. For long, it has been technically easier to study the separation of chromosomes than it was to follow the different steps of cytokinesis. Besides, cancer investigations have mainly focused on the consequences of pathological modifications of any form in nucleic acid sequences than on changes in functional-structural or cellular phenotypes [4]. The relative dependence between mitosis and cytokinesis varies between cell types, but canonically cytokinesis begins with the Spindle Assembly Checkpoint, at the end of which the Anaphase-promoting complex/cyclosome complex (APC/C) degrades Cyclin B, thereby inactivating the Cyclin-dependent kinase 1 (CDK1) [5,6]. The kinases Aurora B and Polo-Like Kinase 1 (PLK1) kinases also contribute

to the initiation of the central spindle assembly [5]. Early cytokinesis corresponds to the contraction of the actomyosin ring perpendicularly to the central spindle microtubules. Then, the stabilisation of the nascent intercellular bridge and the maturation of its central midbody part during late cytokinesis lead to the cytokinetic abscission [6].

Centrosomal Protein 55 (CEP55) is a central regulator during this late stage in human cells, where it participates in midbody structuration and ESCRT machinery recruitment, hence contributing to both the abscission checkpoint and the final disruption of the intercellular bridge [7,8]. Interestingly, CEP55 persists after abscission in midbody remnants, which are degraded either by autophagy or after engulfment reminiscent of phagocytosis, and possibly mediate differential cell fate by asymmetric inheritance [9-12]. CEP55 is stabilised during mitosis by a series of post-translational modifications. It has been shown that CDK1 and Extracellular signal-regulated kinase 2 (ERK2) phosphorylate the S425 and S428 serines, which favours the cis-trans isomerisation of the neighbouring prolines by Peptidyl-prolyl cis-trans isomerase NIMA-interacting 1 (PIN1) [13,14]. These modifications are taking place in a proline-rich linker between two CEP55 Ubiquitin-Binding domains (UBDs) [15]. We have recently reported that the C-terminal Ubiquitin-Binding Zinc-finger (UBZ) is necessary and sufficient to recruit CEP55 to the midbody, whilst the NEMO-Optineurin-ABIN domain (NOA) contributes to post-recruitment abscission [15]. The phosphorylation by PLK1 of serine 436 delays the recruitment of CEP55 until the inhibitor of Apoptosis Stimulating Protein of p53 / Protein Phosphatase 1 complex (iASPP-PP1) dephosphorylates the same serine [16,17].

The role of several phosphorylations is well characterised in cytokinesis, whereas the contribution of the Ubiquitin signaling is not well understood [5,18-21]. Ubiquitin is grafted as a monomer or a chain on substrate proteins to modify their cellular compartment and their assembly, or conversely to promote their proteasomal degradation [22]. Even if other Ubiquitin linkages exist, one roughly distinguishes degradative K48 from non-degradative polyubiquitin M1 and K63 chains [23]. We showed recently that the latter are specifically recognised by CEP55's UBDs, thereby connecting the structural and functional importance of these domains with the cell biology of cytokinesis [15]. Nevertheless, we do not know the ubiquitinated substrate(s) recognised by CEP55, although it is generally accepted that its recruitment depends on Mitotic kinesin-like protein 1 (MKLP1) [13]. Ubiquitination is performed by the consecutive action of E1 Ubiquitin-activating enzymes, E2 Ubiquitin-conjugating enzymes and E3 Ubiquitin ligases, respectively catalysing the activation, conjugation and the ligation of a Ubiquitin monomer usually on a lysin or the initial methionine of a substrate [24,25]. The reverse reaction is catalysed by deubiquitinases (DUB) [26]. Few Ubiquitin ligases and DUBs have been observed at the intercellular bridge or at the midbody, without much, if any, functional description of their structural roles [20,21,27-33]. But a clear description of the Ubiquitin signaling during late cytokinesis has not emerged yet. The quantification of the phenotypes induced by the depletion of CEP55 or the invalidation of its UBDs has given us the opportunity to understand more about this signaling. These interconnected phenotypes include an increased frequency of intercellular bridges and of multinucleation events, a decreased recruitment of CEP55 to the midbody as well as an increased number of midbody remnants per cell. In this report, we screened for Ubiquitin-related enzymes involved in late cytokinesis by RNA interference.

Over time, forward and reverse genetics have given insightful information about cytokinesis in different organisms and cell systems [34-37]. Besides, the emergence of RNA interference has really brought a more detailed understanding of different essential genes involved in cytokinesis [38-43]. This may be more challenging with CRISPR-Cas9-mediated knockout methods where complete disruption of essential genes can affect cell viability [44]. Nevertheless, most if not all the screens focusing on cytokinesis used multinucleation as endpoint readout, thereby only detecting the genes whose downregulation results in the absence of bridge formation or in the collapse of it [38-43]. Indeed, live cell imaging has confirmed that the knockdown of some involved genes does not always lead

to multinucleation, but to an increased duration or length of the intercellular bridge [38,45-48]. Since no method to detect cytokinetic bridges in high-content screening and fixed conditions was available, we decided to code such an image-based tool. After validation, we used it to screen for Ubiquitin-related enzymes by automatically measuring the frequency of cytokinetic bridges.

2. Materials and Methods

Cell lines and cell culture. Human HeLa cells (American Type Culture Collection, CCL2) were cultivated in DMEM supplemented with 10 % heat inactivated FBS and Penicillin/Streptomycin, 100 units/ml and 100 mg/ml respectively.

siRNAs and screening bank. To optimise and test the automated detection of intercellular bridges, we downregulated *CEP55* by separately using several different siRNAs: siGENOME siRNAs D-006893-05-0005 (GGAGAAGAAUGCUUAUCAA), D-006893-06-0005 (UAACACAGUUGGAAUCCUU), D-006893-07-0005 (GAAGAGAAUGA UAUUGCUA), D-006893-08-0005 (GCGAUCUGCUUGUCCAUGU) from Dharmacon and the SI02653021 (CAGGUUAUUGCUAAUGGGUUA) from Qiagen. During this development, scrambled control siRNAs from Dharmacon were employed: siGENOME non-targeting siRNAs D-001210-02-05 (UAAGGCUAUGAAGAGAUAC), D-001210-03-05 (AUGUAUUGGCCUGUAUUAG), D-001210-04-05 (AUGAACGUGAAUUGCUCAA), D-001210-05-05 (UGGUUUACAUGUCGACUAA); siGENOME non-targeting siRNA pool D-001206-13-20 (UAGCGACUAAACACAUCAA, UAAGGCUAUGAAGAGAUAC, AUGUAUUGGCCUGUAUUAG, AUGAACGUGAAUUGCUCAA); ON-TARGETplus non-targeting siRNA pool D-001810-10-20 (UGGUUUACAUGUCGACUAA, UGGUUUACAUGUUGUGUGA, UGGUUUACAUGUUUUCUGA, UGGUUUACAUG UUUUCCUA). Some experimental control conditions were mock-transfected. The human siRNA siGENOME library targeting genes coding for Ubiquitin ligases and deubiquitinases was obtained from Dharmacon (GU-006205-E2-01). The bank was resuspended in siRNA buffer (B-002000-UB-100, Dharmacon) according to instructions given by the manufacturer. During the screening, the negative scrambled control siRNA pool (D-001206-13-20) and the positive controls against *CEP55* (D-006893-05-0005, D-006893-06-0005, D-006893-07-0005, D-006893-08-0005) were randomised on each plate. Validation of the candidate genes was performed with the same individual siGENOME siRNAs targeting respective screening hits: *LNX2* (D-007164-01-0005, CCAAGUGGCUCUUCAUAAA), *UCHL1* (D-004309-01-0005, UAGAUGACAAGGUGA AUUU), *MYSM1* (D-005905-01-0005, GAAGAGAACUGUACAAAGG), *HECW2* (D-007192-01-0005, GCAGAGAUCU-AACUCCAUA), *RNF7* (D-006907-02-0005, UCUUAGA UGUCAAGCUGAA), *RNF157* (D-022965-01-0005, UGAGAAGCCUGGUCAAUAU), *WDR59* (D-022683-01-0005, GAGCUGAAGUGUUGAAGUU), *TRIM25* (D-006585-01-0005, GACCGCAGCUG-CACAAGAA), *RNF13* (D-006944-01-0005, GAAACUUCCUGUA CAUAAA), *VPS8* (D-023668-01-0005, GCAAUAAGCUCCUUGUAUA), *NEURL* (D-016715-01-0005, CCACAAGGCUGUCAAGAGG), all ordered from Dharmacon. The controls during validation of the candidates were the negative scrambled siRNA pool (D-001206-13-20) and a siRNA against *CEP55* (D-006893-05-0005).

Screening and transfection. The bank of siRNAs targeting the genes encoding Ubiquitin ligases and deubiquitinases was randomly distributed in 96 well plates as well as the negative and positive controls per plate. The plate borders were not used to avoid edge effects. Three thousand HeLa cells in 50 µl medium were reverse transfected with 25 nM final siRNA concentration and 0.1 µl DharmaFECT 1 transfection reagent (T-2001-02, Dharmacon). 48 hours post-transfection the cells were fixed with 4 % PFA. During optimisation of the automated detection and during validation of the candidates, the reverse transfection was performed in 24-wp on glass coverslips and the volumes adapted proportionally to reach the same concentrations. To validate the siRNAs and verify the downregulation of candidate genes the reverse transfection was performed in 6-wp and the volumes adapted proportionally to reach the same concentrations.

Immunofluorescence and imaging. The transfected and fixed cells were treated with 50 mM NH_4Cl to reduce autofluorescence before permeabilisation with 0.2 % Triton X100. Once blocked with PBS 1x - 1 % BSA, primary staining was performed one hour at room temperature with the following antibodies: 1:2000 mouse monoclonal anti-β-tubulin (clone TUB 2.1), Sigma-Aldrich (T4026); 1:300 mouse monoclonal anti-CEP55 (clone B8), Santa Cruz Biotechnology (sc-374051); 1:1000 rabbit polyclonal anti-MKLP1 (N-19), Santa Cruz Biotechnology (sc-867). Following washes in PBS 1x, incubation was performed under the same conditions with the secondary antibodies: 1:1000 goat polyclonal anti-mouse IgG1 coupled with AF488 (ThermoFisher Scientific A-21121); 1:1000 goat polyclonal anti-mouse IgG2a coupled with AF546 (ThermoFisher Scientific A-21133); 1:1000 goat polyclonal anti-rabbit coupled with AF647 (ThermoFisher Scientific A-21245). After counterstaining with DAPI, the plates were imaged on the Opera Phenix High-Content Screening system (PerkinElmer), 12 images per well at 20x magnification. Alternatively, coverslips were mounted on slides using Mowiol and images acquired with an Axio Imager Z1 (Carl Zeiss) at the same magnification.

RT-qPCR. Total RNA from transfected HeLa cells was extracted using Nucleospin RNA kit (Macherey Nagel 740955.50) according to the manufacturer's protocol. SYBR Green-based real-time PCR assay (Luna Universal One-Step RT-qPCR Kit, New England Biolabs E3005S) were performed in a final volume of 5 µl per reaction in white ultraAmp 384-well PCR plates using QuantStudio 6 Flex real-time PC system (Applied Biosystems 4485689). Briefly, 2 µl of RNA were added to 2.5 µl of 2X Luna Universal One-Step Reaction Mix and primers (Eurofins Genomics) at a final concentration of 0.4 µM (sequences available on request). The PCR program included a reverse transcription step at 55°C for 10 min, followed by 40 cycles of denaturation at 95°C for 10 s and extension at 60°C for 1 min. SYBR Green fluorescent emission was measured at the end of the elongation step. Subsequently, a melting curve program was applied with a continuous fluorescent measurement starting at 60°C and ending at 95°C (ramping rate of 0.05°C.s^{-1}). Crossing point values (Cp) were determined by the second derivative maximum method in the QuantStudio software. For result normalisation, control genes were tested with the Normfinder program [49]: *Actin B (*Beta Actin*)*, *B2M* (Beta-2 Microglobulin*)*, *GAPDH* (Glyceraldehyde-3-Phosphate Dehydrogenase), *PPIA* (Peptidylprolyl Isomerase A), *HPRT* (Hypoxanthine-Guanine Phosphoribosyltransferase). *PPIA* was selected as the most stable reference gene for the Hela cells. The relative RNA quantities were calculated as follows: $(E_{target})^{\Delta Cp(target)}$ / $(E_{ppia})^{\Delta Cp(PPIA)}$, with E the PCR efficiency of each primer pair and ΔCp the Cp difference between control and sample for each gene [50].

Software development. Our tool to automatically detect intercellular bridges was written in Java as a plugin within the Icy image analysis software [51]. The source code is available in GitLab and Zenodo. The plugin can be downloaded from the Icy website as described in the data availability section. Identification of the midbody, the nucleus and the cytoplasm by detection of the respective signal is required to classify a midbody as part of an intercellular bridge or as remnant. The logic behind this plugin is explained in the results and the discussion.

Image analysis and quantification. All the analyses were executed with the Icy image analysis software with which DAPI-stained nuclei and MKLP1 spots can be automatically detected by the HK-means method. During the development of the image analysis plugin, intercellular bridges were first detected by eye, then the results were compared to those obtained with different versions of the program. An average of a thousand cells was analysed per condition during this initial step. The optimal plugin, whose code is available, was applied for screening, where an average of two hundred and fifty cells were analysed per condition. During the screen, the frequency F of intercellular bridges was estimated by F = I / (N – I) * 100, where the number of cells is calculated by subtracting the number of cytokinetic bridges I to the number of nuclei N in the condition. The validation of the candidates was performed by manually and blindly counting the frequency of cytokinetic bridges in an average of two hundred and fifty cells per replicate. The number

of multinucleated cells counted manually was also subtracted to the number of nuclei during the validation of the candidates, since the multinucleation phenotype was measured concomitantly. The frequency F′ of intercellular bridges became then F′ = I / (N – I – M) * 100, where M is the number of multinucleated cells. Similarly, the frequency F′′ of multinucleated cells was estimated by F′′ = M / (N – I – M) * 100. The recruitment of CEP55 to the midbody was evaluated by measuring within each MKLP1 spot the average intensity ratio of the CEP55 to the MKLP1 signal. The number of midbody remnants was estimated by subtracting the number of intercellular bridges to the number of MKLP1 spots. Then the number of midbody remnants per cell was calculated and expressed as a percentage.

Representation and statistical analysis. Data were represented and statistics were calculated with R. The Spearman's rank correlation coefficient was estimated to evaluate the performance of the automated detection of intercellular bridges. To get an idea of the statistical strength of an effect during the screen, the z-score was calculated for each tested siRNA by $z = (x - \mu) / \sigma$, where μ and σ are respectively the average frequency and the standard deviation of intercellular bridges in all the tested wells from the plate where this siRNA was transfected, and where x is the frequency of cytokinetic bridges in this specific well. Hits were selected based on the z-score and the frequency of intercellular bridges. The validation of candidate genes with different CEP55-related phenotypes was verified by adjusted Wilcoxon-Mann-Whitney tests comparing the distribution of the replicates for each hit with those obtained with the non-targeting scrambled siRNA pool. Images and graphical representations were assembled with the Inkscape software.

3. Results

3.1. Development of an automated detection of cytokinetic bridges

Taking benefits from the environment of the Icy image analysis software, we developed a plugin written in Java to automatically detect intercellular bridges. To this aim, we first had to detect the different types of biological object before interrogating their relationships. The preliminary step was to determine optimal and robust immunofluorescence staining conditions for each relevant type of object. DAPI and β-tubulin are frequently used to stain nuclei and cytoplasms respectively. As part of the Centralspindlin complex, MKLP1 is one of the earliest elements of the midbody and mediates the recruitment of CEP55, which highlights its relevance as a marker for the midbody. Staining and imaging conditions were easily calibrated and are summarised in the methods (Figure 1).

To detect nuclei and midbodies, we applied HK-Means combining hierarchical clustering with K-Means methods [52]. This segmentation method executes an N-class thresholding based on a K-Means classification of pixels from the histogram of their intensities in the image, before extracting regions of interest (ROI) in a bottom-up manner following parameters defined by the user, i.e. minimum and maximum size of the clustered object as well as its minimum intensity. This allowed us to easily count the number of nuclei and the number of midbodies per field of view (FOV) and per condition. The boundaries of the detected nuclei were refined by progressively fitting the contour of each nuclear ROI to the nuclear shape, following an active contouring method based on intensity gradient and edge detection [53]. Each midbody spot was expanded by a constant user-defined number of pixels in order to draw a larger spot, from which the initial one was subtracted, hence generating a midbody ring. Given that the cytoplasms of future daughter cells remain connected until abscission, we decided to avoid their segmentation. We simply generated a single region of interest per image encompassing all detected cytoplasms. This cytoplasmic ROI was drawn by automated thresholding using K-Means, where the number of intensity classes to determine the minimum positivity threshold is user-defined (Figure 1a and 1b).

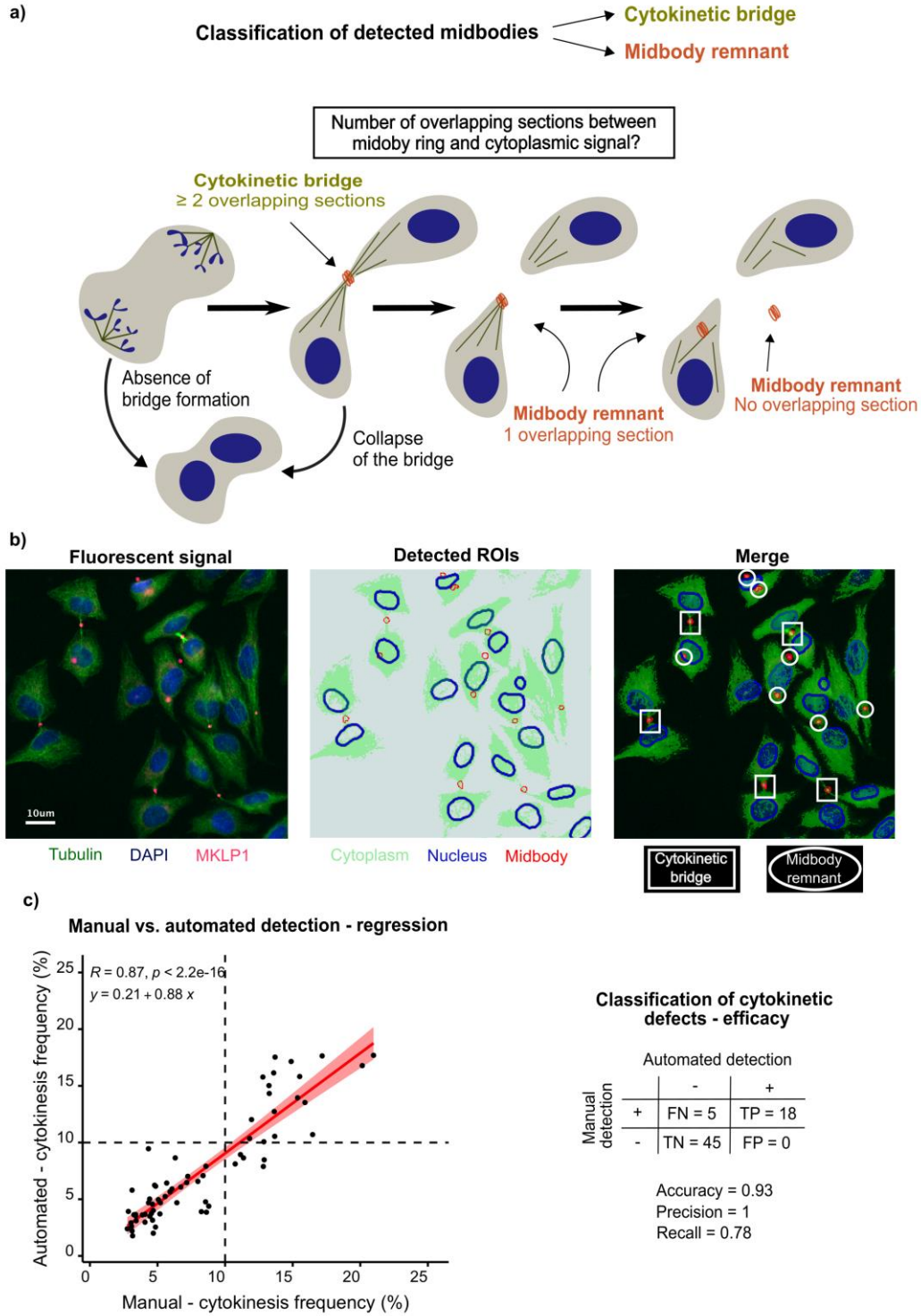

Figure 1. Development of the automated detection of intercellular bridges. (a) Unlike the observation of multinucleation, the detection of intercellular bridges is a more appropriate phenotype to study late cytokinesis. A midbody present at the intercellular bridge is connected to each future daughter cell, whereas a midbody remnant is observed within one cytoplasm or outside cells. To classify each midbody, we detected the number of overlapping sections between each drawn surrounding midbody ring and the cytoplasmic ROI. (b) All three necessary elements to classify midbodies were delineated by automated detection of respective signals in HeLa cells: DAPI for nuclei (blue), β-tubulin for cytoplasms (green) and MKLP1 for midbodies (red). The image on the right is the overlay of the merged signals and the detected regions of interest, i.e. left and middle image respectively. The colour code is maintained between the detected signals and the represented ROIs.

On the overlay, examples of detected midbodies classified as cytokinetic bridges (rectangles) or midbodies (ovals) are highlighted. (c) Performance of the bioimage analysis tool in HeLa cells. Left, the frequencies of cytokinetic bridges from a blind manual detection of intercellular bridges were plotted against those obtained automatically by the program. The dots represent 68 experimental conditions from four different experiments. In each condition, cells were transfected either with an siRNA targeting *CEP55*, a non-targeting scrambled siRNA or mock-transfected. The correlation between the results of the two methods was appreciated by a Spearman correlation test. The vertical dashed line corresponds to a threshold which separated the mock-transfected and the conditions transfected with a scrambled siRNA from the conditions transfected with an siRNA targeting *CEP55*: blindly and manually measured, their cytokinesis frequency was always found exclusively below or above 10 % respectively. The same threshold was applied for the automated detection of cytokinetic bridges and represented by a horizontal dashed line. Right, the efficacy of the classification was estimated based on these thresholds, while considering manual counting as the gold standard. The number of true (TP) or false (FP) positive and of true (TN) or false (FN) negative results of the classification allowed the calculation of performance parameters such as accuracy, precision and recall.

Once delineated, we interrogated the relations between nuclear, midbody and cytoplasmic ROIs to estimate the number of cytokinetic bridges. Midbodies were either classified as remnants or as intercellular cytokinetic bridges. The ring surrounding each midbody spot was examined to establish how many times it was crossing the β-tubulin signal and if it was intersecting with any DAPI-positive ROI. Midbody rings with a single intersection or without any interaction with the cytoplasmic ROI were classified as midbody remnants. When at least two intersections were counted, the midbody was considered as part of a cytokinetic bridge. If the ring was intersecting with or inscribed in a nucleus, the midbody was classified as remnant (Figure 1a). In terms of output, the plugin overlays all the detected ROIs on each respective image of a sequence (Figure 1b). Per field of view and per condition, the number of nuclei, the number of midbodies and the number of cytokinetic bridges as well as the criteria for the classification of each midbody are exported. The plugin and the code are accessible as described in the data availability section.

To evaluate the accuracy of the automated detection, we compared its results with those of a preliminary blind manual detection in a set of 68 conditions from four different experiments, with an average of 1000 analysed cells for each condition (Figure 1c). In each one, HeLa cells were mock-treated or transfected with one of several anti-*CEP55* or scrambled non-targeting siRNAs at 25 nM. The number of detected cytokinetic bridges was subtracted to the number of nuclei to estimate the number of cells. The frequency of cytokinetic bridges was then calculated per condition and expressed as a percentage. Manually, the frequency of cytokinetic bridges in mock-transfected conditions and in those treated with a scrambled siRNA was measured below 10 %. Upon downregulation of *CEP55* with an siRNA, the cytokinesis frequency was consistently measured above 10 %. This is the reason why we chose 10 % as the threshold to evaluate the accuracy of the classification by the automated image analysis tool. Each software version was similarly tested until we were satisfied with the accuracy of the detection. The current and herein described version of the software showed the best performance with a Spearman correlation coefficient of 0.87. The linear correlation was attested by a visually rather linear distribution of the data and a significant result of the correlation test with $p < 10^{-15}$. With $R^2 = 0.75$, three quarter of the observed variation can be explained by the correlation. The parameters of the affine function summarising the correlation curve were the slope a = 0.88 and the translation b = 0.21. By applying the threshold of 10 % to the results of the automated detection, we were able to evaluate the performance of the classification. In brief, the accuracy of the software was equal to 0.93. The precision and recall values were 1 and 0.78 respectively. Taken together, the accuracy of the automated detection of intercellular cytokinetic bridges allowed us to screen for Ubiquitin-related enzymes in late cytokinesis.

In the supplementary Figure S1, we show the performance of the detection of cytokinetic bridges by the software in WT and *CEP55* KO U2OS cell lines. We have already

published with these cell lines. The software could easily classify the cell type based on the frequency of cytokinetic bridges. However, the detection was not optimal, as the slope of the regression was close to 0.5. Firstly, this was due to the fact that the cytokinetic bridges in these cells are not as long as in HeLa cells. Secondly, the environment of each individual cell is rather crowded since U2OS cells grow in small colonies. Thus, we decided to work with HeLa cells in which the effect of gene downregulation was more efficiently detected. Nevertheles, these results have increased our confidence in the robustness of our tool.

3.2. Screening of Ubiquitin ligases and deubiquitinases involved in late cytokinesis

To address a relevant biological question with our image analysis tool, we screened a library of siRNAs targeting Ubiquitin ligases or DUBs to detect their involvement in late cytokinetic steps (Figure 2). We applied the same experimental conditions as during optimisation of the automated detection, i.e. a 48 hour-long incubation after transfection of 25 nM siRNA. The position of the tested siRNAs was randomised on 96-well plates, each of them including controls. Positive controls were treated with four different siRNAs against *CEP55*. Negative controls were either mock-treated or transfected with scrambled non-targeting siRNAs (Figure 3a). Since we inconsistently reached a positive z'-factor between positive and negative controls during the screening setup, we only used these conditions as experimental controls for each plate and to evaluate the consistency between plates. As planned, wells at the edge of each plate were avoided to prevent border effects. The staining and analysis conditions were concordant with those used during optimisation.

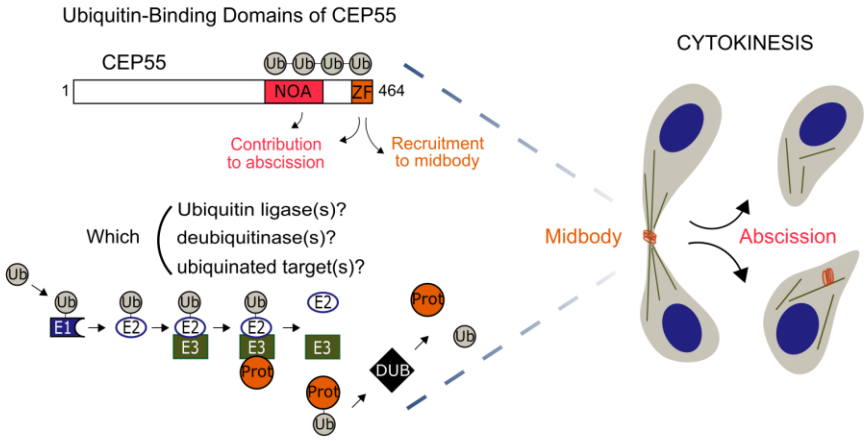

Figure 2. Descriptive diagram of the raised biological questions. CEP55 is a key actuator of late cytokinesis. The Zinc-finger (ZF) domain in CEP55 cargoes the protein to the midbody, whereas NOA contributes to the cytokinetic abscission. The presence of these two functional Ubiquitin-Binding Domains in CEP55 structurally links the Ubiquitin signaling with late cytokinesis. Ubiquitination requires three successive reactions named activation, conjugation and ligation, catalysed respectively by E1, E2 and E3 Ubiquitin enzymes. Ubiquitin architectures are edited or withdrawn from substrates by deubiquitinases. Such molecular actors are not known regarding the recruitment of CEP55 to the midbody and its late cytokinetic function, i.e. abscission and recycling of the midbody remnants.

671 genes encoding either a Ubiquitin ligase or a deubiquitinase were targeted across all thirteen plates, with at least six positive or negative controls per plate. An average of 250 cells were analysed per condition. The frequency of intercellular cytokinetic bridges was the endpoint readout to estimate the occurrence of late cytokinetic events. Across plates the downregulation of *CEP55* by the different positive control siRNAs led to an

increase in the frequency of intercellular bridges to 17.48 +/- 4.01 % (mean +/- SD). In contrast, the average frequency of cytokinetic bridges was 6.04 +/- 1.90 % in the wells treated with scrambled non-targeting siRNAs and 6.29 +/- 1.73 % in the mock-treated conditions. We did not observe any plate effect. An 11 % positivity threshold of cytokinesis frequency was set, above which hits were selected (Figure 3b). We calculated a z-score per tested siRNA based on the mean and the standard deviation of all the tested siRNAs on the same plate (supplementary Figure S2). This score and the available literature have guided us to narrow the selection down to eleven hits, whose downregulation increased the frequency of cytokinetic bridges. These hits are listed by the name of the targeted gene, associated with the respective observed frequency of intercellular bridges: *UCHL1*, 16.51 %; *NEURL*, 16.29 %; *TRIM25*, 15.60%; *WDR59*, 13.85%; *RNF7*, 13.81; *HECW2*, 12.64 %; *LNX2*, 12.20 %; *MYSM1*, 11.45 %, *RNF157*, 11.40 %; *RNF13*, 11.31%; *VPS8*, 11.11 %. In total 1.64 % of the targeted genes were considered positive after this initial screen. The results obtained with all the tested siRNAs from the library are available in the supplementary Table S1.

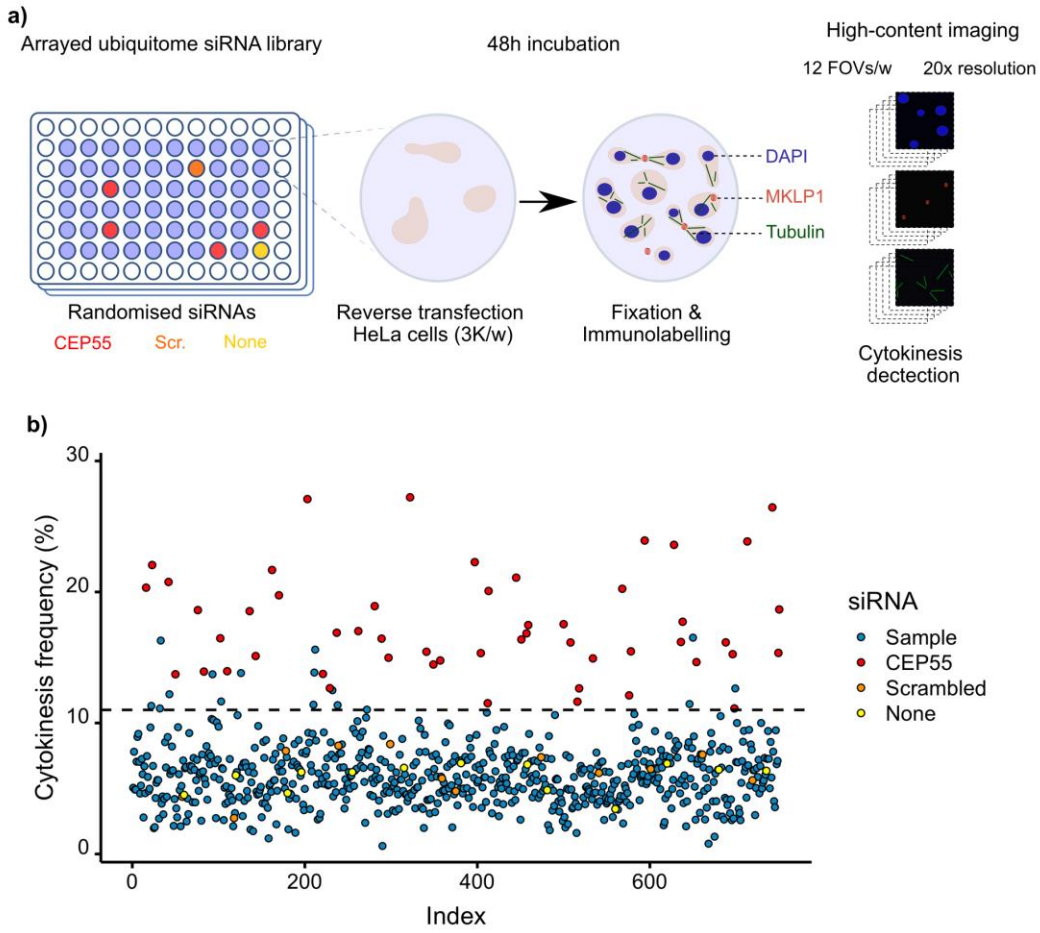

Figure 3. Overview of the screening execution. (a) Representation of the screening pipeline from the plate map until imaging. (b) The distribution of the screening results indexed according to their chronological order of acquisition does not show any plate effect. The dashed line represents the positivity threshold above which samples were considered as hits.

3.3. Validation of the screening based on CEP55-related phenotypes

As described in our recent publication, the downregulation of *CEP55* leads to four different phenotypes (Figure 4). The increase in the frequency of intercellular bridges and in multinucleation results from the inhibition of late cytokinesis, due to the lack of CEP55 at the midbody [7,13]. This absence also results in the increase in the number of midbody

remnants per cell, possibly due to the lack of midbody recycling, either through autophagy or lysosomal degradation after engulfment [9-11]. These interconnected phenotypes appear when CEP55's Ubiquitin-Binding Domains are debilitated. Therefore, we expected phenocopies when downregulating some Ubiquitin-related enzymes. As part of the validation of the primary screen, we blindly evaluated the presence of these same phenotypes under downregulation of the different hit genes with respective siRNAs (Figure 5). For each hit, six biological replicates were performed in HeLa cells under the same conditions of downregulation as during the screen, i.e. 48 hours post-transfection with 25 nM siRNA. An average of 250 cells were analysed per replicate. Downregulation of *CEP55* was established as the positive control, while the negative scrambled control was the reference for the statistical tests.

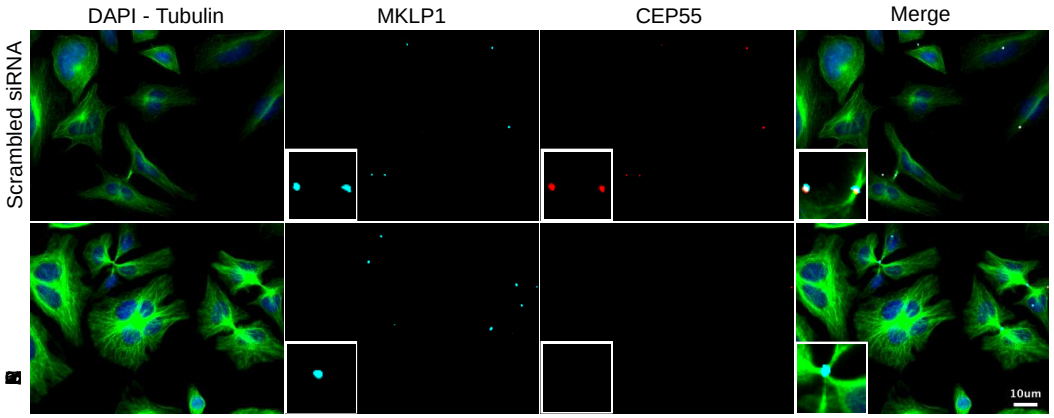

Figure 4. Phenotypes induced by the downregulation of *CEP55*. Immunofluorescence images of HeLa cells 48 hours post-transfection either with 25 nM non-targeting scrambled or anti-*CEP55* siRNA. The identification of nuclei, cytoplasms and midbodies was enabled by staining with DAPI, anti-β-tubulin and anti-MKLP1 antibodies. The staining of CEP55 allows the evaluation of its expression and its recruitment to the midbody. Insets correspond to a 4-fold magnified view of a region in the respective image.

Targeting the Ligand of Numb-protein X 2 (*LNX2*) or the Neuralised E3 Ubiquitin protein ligase 1 (*NEURL*) resulted in a reproducible significant increase in the frequency of cytokinetic bridges (Figure 5a). More multinucleated cells were observed when knocking down the Ring Finger protein 157 (*RNF157*) or *NEURL* (Figure 5b). The downregulation of the Ring Finger protein 13 (*RNF13*), *RNF157*, *LNX2* or the Ubiquitin C-terminal Hydrolase 1 (*UCHL1*) variably reduced the intensity of the CEP55 signal at the midbody (Figure 5c). When *RNF157* or LNX2 was knocked down the number of midbody remnants decreased relative to the number of cells, whereas the number of remnants per cell increased after downregulation of *UCHL1* (Figure 5d).

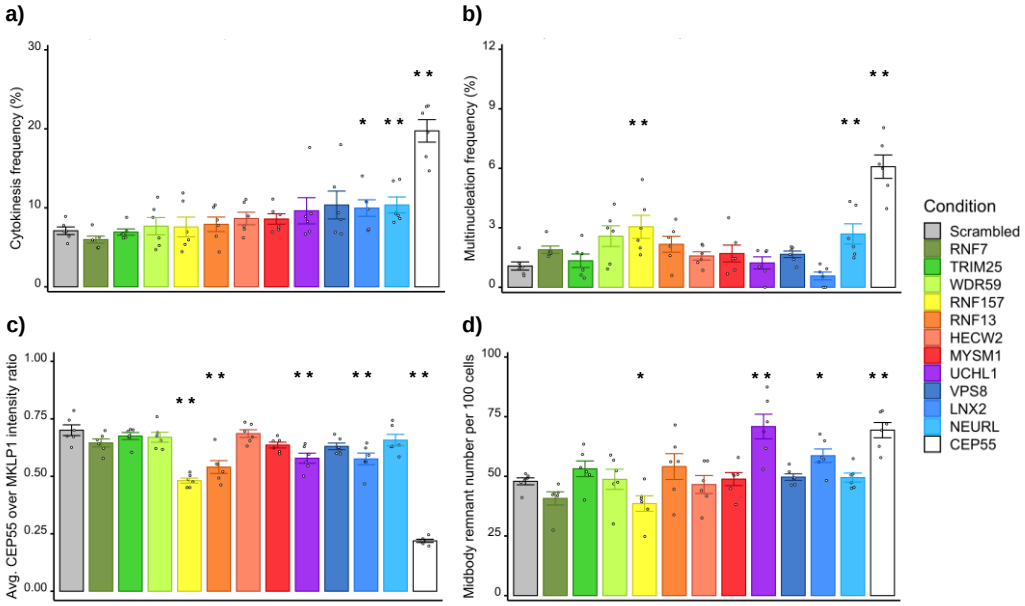

Figure 5. Validation of candidate genes by measurement of CEP55-related phenotypes. HeLa cells were transfected 48 hours with 25 nM of siRNA against each selected and color-coded hit. (a) Frequency of cytokinetic bridges. (b) Frequency of multinucleated cells. (c) Average intensity ratio of CEP55 to MKLP1 signals per midbody. (d) Number of midbody remnants per 100 cells. Per condition, mean and standard error are represented as well as individual replicates. For each condition, six biological replicates were performed. The total number of cells and the total number of midbodies analysed in all replicates are respectively shown in (a) and (c). Wilcoxon-Mann-Whitney tests compare the distributions of the replicates, where the scrambled siRNA condition is the reference. * $p < 0.05$; ** $p < 0.01$; *** $p < 0.001$.

While extending the frame of the primary screen through the consideration of new readouts, we decided to preserve reasonable stringency and to select only candidates whose downregulation alters at least two of the CEP55-related phenotypes. Thus, these data allowed the validation of *LNX2*, *NEURL*, *UCHL1* and *RNF157*. Complementary results shown in the supplementary Figure S3 validate the efficient and specific downregulation these candidates as well as *CEP55* by siRNA. Despite our careful demonstration, caution should be taken until cross-validation using an alternative method to RNA interference during the exploration of each remaining candidate gene, as we used only one siRNA per gene. To illustrate the direct effect of their downregulation on the recruitment of CEP55 to the midbody, representative images are shown in Figure 6. Altogether, our results help the detection of late cytokinetic events and contribute to the understanding of the Ubiquitin signaling linked to CEP55 and cytokinetic abscission.

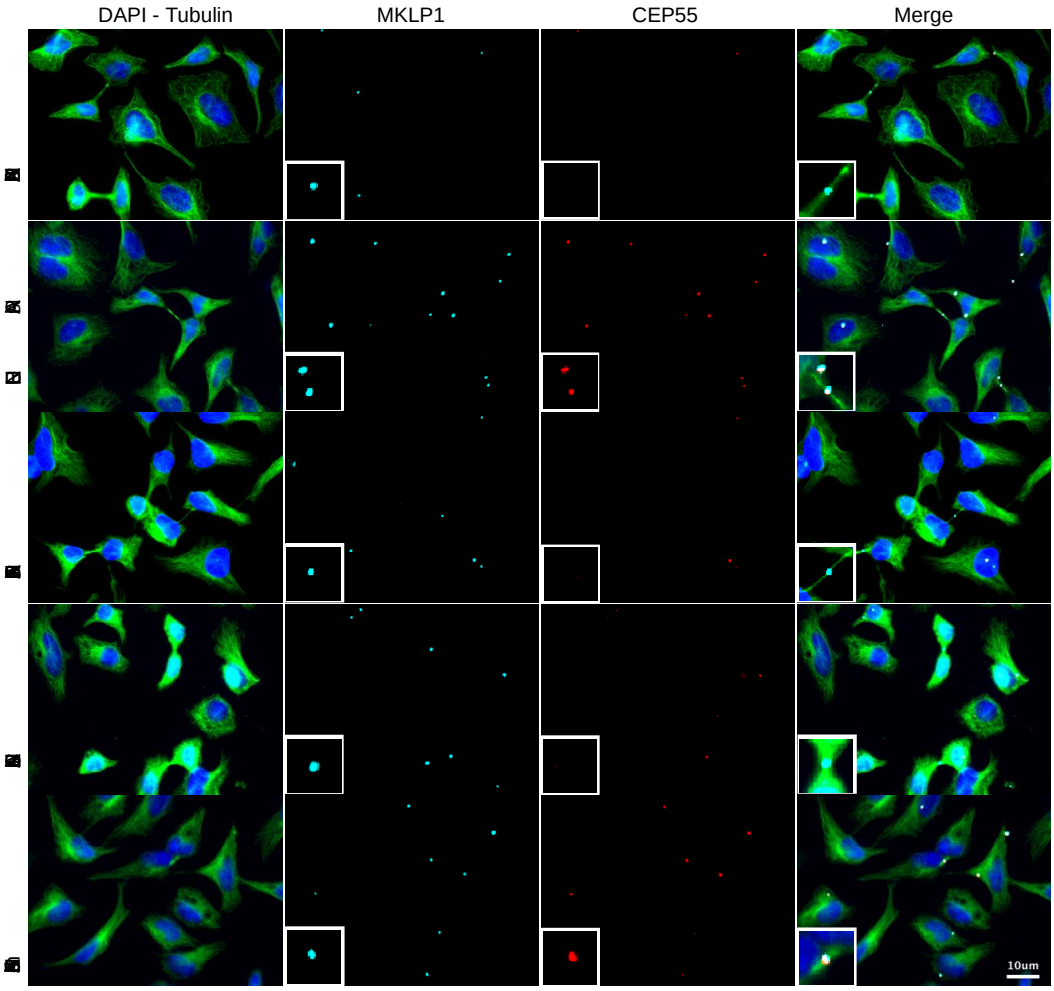

Figure 6. Representative phenotypes observed in validated candidates. Immunofluorescence images of HeLa cells 48 hours post-transfection either with 25 nM non-targeting or anti-candidate siRNA. The identification of nuclei, cytoplasms and midbodies was enabled by staining with DAPI, anti-β-tubulin and anti-MKLP1 antibodies respectively. The staining of CEP55 allows the evaluation of its expression and its recruitment to the midbody. Insets correspond to a 4-fold magnified view of a region in the respective image.

4. Discussion

Since previous cytokinetic screens relied on the detection of multinucleated cells, our first technical aim was to enable the endpoint detection of intercellular cytokinetic bridges. The constant improvement of mathematical functions to detect standard biological objects in microscopic images has allowed us to write a plugin within the environment of the Icy image analysis software. This plugin first recognises the stained nuclei, cytoplasms and midbodies, before classifying the latter as remnants or as part of cytokinetic bridges. The performance of the automated detection in HeLa and U2OS cells gives us confidence in our ability to detect and classify the same structures in other fixed cell lines or even in primary cells. This tool will become very useful to identify active compounds or any biochemical modifier that blocks the late cytokinetic events leading to abscission. However, this method may underestimate the impact of some perturbations in cytokinesis. Indeed, inhibiting cytokinesis frequently leads to the absence of cytokinetic bridge or its collapse, both leading to multinucleation and likely to cell death through incompletely characterised molecular mechanisms [45,54,55]. Nevertheless, the reliable detection of intercellular bridges might be useful to perform High-Content Screening of late cytokinetic events. This would balance the low throughput of live imaging, which is usually employed to study the duration of cytokinesis especially the last steps leading to abscission [38,48]. Here, we

used this approach to screen for Ubiquitin ligases and DUBs involved at this stage of the cell cycle.

The screen was carried out despite the statistically limited difference between positive and negative controls, but the setup, execution and analysis were eased by our technical development. The threshold of positivity for hits as well as the z-scores gave us reasonable confidence in our screen. Based on the knowledge accumulated in our previous publication about CEP55's UBDs, we decided to validate the hits whose downregulation alters at least two CEP55-related phenotypes [15]. While the downregulation of *CEP55* reached nearly 100%, the downregulation of the gene candidates was slightly less efficient with a minimum of 80% (supplementary Figure S3).

However, *NEURL* and *LNX2* were increasing the frequency of intercellular bridges upon knockdown. In *D. melanogaster*, NEUR ubiquitinates the ligand Delta and Jagged to promote its endocytosis, hence inducing the Notch signal in *trans [56,57]*. In mammalians, the contribution of its homolog NEURL to this function in the Notch pathway appears to be complemented by MIB1, whose downregulation did not alter the frequency of cytokinetic bridges in our screen [56,57]. It should be noted that the lack of phenotypic effect observed with MIB1 could be due to the presence of several functional and redundant genes in mammalian cells. LNX2 is also known to target Numb for proteasomal degradation, hence influencing the Notch signaling in *cis* [58,59]. However, the role of Notch in cytokinesis has never been highlighted, despite clearly modulating the fate of daughter cells during asymmetric division [60]. While a putative link could be established between late cytokinesis and Notch signaling, other hypotheses need to be drawn, mainly because targeting MIB1 did not show any effect in our screen [61]. NEURL may have other functions for which the ligands are unknown [62]. The downregulation of *NEURL* increased both the frequency of cytokinetic bridges and multinucleated cells, which is clearly in favour of a role in cytokinesis. In the case of LNX2, the number of specific protein substrates for ubiquitination is steadily growing. Both LNX2 and its paralog LNX1 trigger degradative Ubiquitin signal, which does not explain how the depletion of LNX2 could directly decrease the recruitment of CEP55 to the midbody [63,64]. It is rather possible that CEP55 is not recruited to the midbody because of its disorganisation, likely concomitant with the degradation of its protein components. LNX1 and LNX2 are structurally similar and display common protein substrates for ubiquitination [59,63,65]. Recently, proteomic studies have evidenced their potential substrates such as MID1 and MID2 as well as KIF14 [66]. The first two are involved in early cytokinesis, whereas the latter participates in the stabilisation of the central spindle, hence in the structuration of the intercellular cytokinetic bridge [31,67].

The results about UCHL1 are noteworthy, though not directly linked to cytokinetic bridges. Indeed, CEP55 could be associated with the ubiquitinated target leading to the recycling of the midbody. The downregulation of *UCHL1* led to a reduced intensity of CEP55 on midbodies and to an increased number of midbody remnants per cell. Both effects may be in favor of a lack of Ubiquitin chain edited by UCHL1 on a substrate of the midbody. The recycling of midbodies may also be altered by directly disturbing autophagy [68]. Indeed, it has been reported that CEP55 interferes with the formation of LC3-positive autophagosomes [69]. As for RNF157, the two observed effects, i.e. the reduced intensity of CEP55 at the midbody and the increased frequency of multinucleated cells may be more difficult to explain. It is known that the downregulation of *RNF157* induces apoptosis in neuronal cells through a mechanism implicating Fe65, and that it participates to the editing of dendrites [70]. RNF157 was also described as a downstream effector of the PI3K and MAPK pathways [71]. In our hands, the total number of cells was significantly decreased during downregulation of *RNF157*, possibly by apoptosis. Interestingly, the downregulation of *CEP55* in zebrafish leads to massive apoptosis of neural structures concomitantly with a reduced AKT activation [72]. Besides, CEP55 is phosphorylated by the ERK2 kinase [13]. Nevertheless, these theoretical analogies linking CEP55 with RNF157 require further experimentations, especially since the hydranencephaly of the

MARCH syndrome is associated with a defect in the recruitment of CEP55 to the midbody [73].

To conclude, we repeat that we should use our tool for screening. Nowadays, cytokinesis remains less understood than mitosis, although cytoplasmic division contributes equally to genome integrity. Specifically, the regulated rupture of the intercellular bridge needs to be understood so that we can imagine blocking it in various types of cancer. As reported in the discussion section of our previous article, we are still looking for elements which condensate the midbody to a state of liquid-liquid phase transition, and we have previously observed Ubiquitin at the midbody. Therefore, we have used our bioimage analysis tool to look for elements of the Ubiquitin signaling system whose downregulation affects cytokinesis. Each candidate gene should be further investigated using an alternative method to siRNA knockdown such as CRISPR interference or some knockout method. Even if we did not deeply characterise the functional role of each candidate gene that results from our siRNA screening, we strongly believe that the replication of cytokinetic defects and the co-occurrence of other CEP55-related phenotypes upon the downregulation of candidate genes in multiple validation experiments strengthen our approach. Indeed, our discovery of functional Ubiquitin-Binding Domains in CEP55 was the main reason why we decided to perform a late cytokinesis screen to search for Ubiquitin-related enzymes which could be associated with the function of CEP55 during and after cytokinesis. In the future, it may also be primordial to investigate the role of these cytokinetic elements in healthy primary cells.

Supplementary Materials: The following supporting information can be downloaded at: www.mdpi.com/xxx/s1. Table S1: Screening data. Indexed results for each tested siRNA. Information about the identity of the targeted genes is available as well as their position in the bank and in the screening plates. The number of cells and detected cytokinetic bridges are reported. The frequency of cytokinetic bridges and the z-score are calculated for each targeted gene. Figure S1: Performance of the bioimage analysis tool in WT and *CEP55* KO U2OS cells. Figure S2: Z-score distribution of the screening results ranked by z-score. Figure S3**:** Specific siRNA knockdown of *cep55* and candidate genes.

Author Contributions: Conceptualization, M.B., L.D. and F.A.; methodology, M.B., L.D. and F.A.; software, M.B.; validation, M.B., K.N.S.H., S.G. and E.G.; formal analysis, M.B. and L.D.; investigation, M.B. and L.D.; resources, M.H. and F.A.; data curation, M.B. and L.D.; writing—original draft preparation, M.B.; writing—review and editing, M.B. and F.A.; visualization, M.B and L.D.; supervision, M.H. and F.A.; project administration, F.A.; funding acquisition, F.A. All authors have read and agreed to the published version of the manuscript.

Funding: This research was supported by a funding from the Global Care Initiative provided by the Carnot Human Health Institute given to LD and FA [ANR-11-CNRT-04]. KNSH was supported by a Ligue Nationale Contre le Cancer fellowship. A PhD fellowship from the Ministère de l'Enseignement Supérieur, de la Recherche et de l'Innovation was attributed to MB. The APC was funded by the Institut Pasteur.

Institutional Review Board Statement: Not applicable.

Informed Consent Statement: Not applicable.

Data Availability Statement: The source code is available in the GitLab (https://gitlab.pasteur.fr/pfccb/cytokinesis) and Zenodo (https://zenodo.org/record/5562194) repositories. and the plugin can be downloaded from the website of the open-source Icy image analysis software (http://icy.bioimageanalysis.org/plugin/cytokinetic-bridge-detector).

Acknowledgments: The authors wish to thank A. Dufour and S. Dallongeville from the Unité d'Analyse d'Images Biologiques headed by J.-C. Olivo-Marin for their help in writing and editing the plugin to detect intercellular cytokinetic bridges. We thank A. Schouwenburg for his careful corections to the manuscript.

564 **Conflicts of Interest:** The authors declare no conflict of interest. The funders had no role in the
565 design of the study; in the collection, analyses, or interpretation of data; in the writing of the manu-
566 script, or in the decision to publish the results.

References

1. Scholey, J.M.; Brust-Mascher, I.; Mogilner, A. Cell division. *Nature* **2003**, *422*, 746-752, doi:10.1038/nature01599.
2. McIntosh, J.R. Mitosis. *Cold Spring Harb Perspect Biol* **2016**, *8*, doi:10.1101/cshperspect.a023218.
3. Pollard, T.D.; O'Shaughnessy, B. Molecular Mechanism of Cytokinesis. *Annu Rev Biochem* **2019**, *88*, 661-689, doi:10.1146/annurev-biochem-062917-012530.
4. Roos, W.P.; Thomas, A.D.; Kaina, B. DNA damage and the balance between survival and death in cancer biology. *Nat Rev Cancer* **2016**, *16*, 20-33, doi:10.1038/nrc.2015.2.
5. Holder, J.; Poser, E.; Barr, F.A. Getting out of mitosis: spatial and temporal control of mitotic exit and cytokinesis by PP1 and PP2A. *FEBS Lett* **2019**, *593*, 2908-2924, doi:10.1002/1873-3468.13595.
6. Mierzwa, B.; Gerlich, D.W. Cytokinetic abscission: molecular mechanisms and temporal control. *Dev Cell* **2014**, *31*, 525-538, doi:10.1016/j.devcel.2014.11.006.
7. Zhao, W.M.; Seki, A.; Fang, G. Cep55, a microtubule-bundling protein, associates with centralspindlin to control the midbody integrity and cell abscission during cytokinesis. *Mol Biol Cell* **2006**, *17*, 3881-3896, doi:10.1091/mbc.e06-01-0015.
8. Petsalaki, E.; Zachos, G. An ATM-Chk2-INCENP pathway activates the abscission checkpoint. *J Cell Biol* **2021**, *220*, doi:10.1083/jcb.202008029.
9. Ettinger, A.W.; Wilsch-Bräuninger, M.; Marzesco, A.M.; Bickle, M.; Lohmann, A.; Maliga, Z.; Karbanová, J.; Corbeil, D.; Hyman, A.A.; Huttner, W.B. Proliferating versus differentiating stem and cancer cells exhibit distinct midbody-release behaviour. *Nat Commun* **2011**, *2*, 503, doi:10.1038/ncomms1511.
10. Kuo, T.C.; Chen, C.T.; Baron, D.; Onder, T.T.; Loewer, S.; Almeida, S.; Weismann, C.M.; Xu, P.; Houghton, J.M.; Gao, F.B.; et al. Midbody accumulation through evasion of autophagy contributes to cellular reprogramming and tumorigenicity. *Nat Cell Biol* **2011**, *13*, 1214-1223, doi:10.1038/ncb2332.
11. Crowell, E.F.; Gaffuri, A.L.; Gayraud-Morel, B.; Tajbakhsh, S.; Echard, A. Engulfment of the midbody remnant after cytokinesis in mammalian cells. *J Cell Sci* **2014**, *127*, 3840-3851, doi:10.1242/jcs.154732.
12. Addi, C.; Presle, A.; Frémont, S.; Cuvelier, F.; Rocancourt, M.; Milin, F.; Schmutz, S.; Chamot-Rooke, J.; Douché, T.; Duchateau, M.; et al. The Flemmingsome reveals an ESCRT-to-membrane coupling via ALIX/syntenin/syndecan-4 required for completion of cytokinesis. *Nat Commun* **2020**, *11*, 1941, doi:10.1038/s41467-020-15205-z.
13. Fabbro, M.; Zhou, B.B.; Takahashi, M.; Sarcevic, B.; Lal, P.; Graham, M.E.; Gabrielli, B.G.; Robinson, P.J.; Nigg, E.A.; Ono, Y.; et al. Cdk1/Erk2- and Plk1-dependent phosphorylation of a centrosome protein, Cep55, is required for its recruitment to midbody and cytokinesis. *Dev Cell* **2005**, *9*, 477-488, doi:10.1016/j.devcel.2005.09.003.
14. van der Horst, A.; Khanna, K.K. The peptidyl-prolyl isomerase Pin1 regulates cytokinesis through Cep55. *Cancer Res* **2009**, *69*, 6651-6659, doi:10.1158/0008-5472.Can-09-0825.
15. Said Halidi, K.N.; Fontan, E.; Boucharlat, A.; Davignon, L.; Charpentier, M.; Boullé, M.; Weil, R.; Israël, A.; Laplantine, E.; Agou, F. Two NEMO-like Ubiquitin-Binding Domains in CEP55 Differently Regulate Cytokinesis. *iScience* **2019**, *20*, 292-309, doi:10.1016/j.isci.2019.08.042.
16. Bastos, R.N.; Barr, F.A. Plk1 negatively regulates Cep55 recruitment to the midbody to ensure orderly abscission. *J Cell Biol* **2010**, *191*, 751-760, doi:10.1083/jcb.201008108.
17. Gao, K.; Zhang, Y.; Shi, Q.; Zhang, J.; Zhang, L.; Sun, H.; Jiao, D.; Zhao, X.; Tao, H.; Wei, Y.; et al. iASPP-PP1 complex is required for cytokinetic abscission by controlling CEP55 dephosphorylation. *Cell Death Dis* **2018**, *9*, 528, doi:10.1038/s41419-018-0561-6.
18. Gilberto, S.; Peter, M. Dynamic ubiquitin signaling in cell cycle regulation. *J Cell Biol* **2017**, *216*, 2259-2271, doi:10.1083/jcb.201703170.

19. Basant, A.; Glotzer, M. Spatiotemporal Regulation of RhoA during Cytokinesis. *Curr Biol* **2018**, *28*, R570-r580, doi:10.1016/j.cub.2018.03.045.
20. Mukai, A.; Mizuno, E.; Kobayashi, K.; Matsumoto, M.; Nakayama, K.I.; Kitamura, N.; Komada, M. Dynamic regulation of ubiquitylation and deubiquitylation at the central spindle during cytokinesis. *J Cell Sci* **2008**, *121*, 1325-1333, doi:10.1242/jcs.027417.
21. Pohl, C.; Jentsch, S. Final stages of cytokinesis and midbody ring formation are controlled by BRUCE. *Cell* **2008**, *132*, 832-845, doi:10.1016/j.cell.2008.01.012.
22. Oh, E.; Akopian, D.; Rape, M. Principles of Ubiquitin-Dependent Signaling. *Annu Rev Cell Dev Biol* **2018**, *34*, 137-162, doi:10.1146/annurev-cellbio-100617-062802.
23. Komander, D.; Rape, M. The ubiquitin code. *Annu Rev Biochem* **2012**, *81*, 203-229, doi:10.1146/annurev-biochem-060310-170328.
24. Pickart, C.M. Mechanisms underlying ubiquitination. *Annu Rev Biochem* **2001**, *70*, 503-533, doi:10.1146/annurev.biochem.70.1.503.
25. Ciechanover, A.; Ben-Saadon, R. N-terminal ubiquitination: more protein substrates join in. *Trends Cell Biol* **2004**, *14*, 103-106, doi:10.1016/j.tcb.2004.01.004.
26. Mevissen, T.E.T.; Komander, D. Mechanisms of Deubiquitinase Specificity and Regulation. *Annu Rev Biochem* **2017**, *86*, 159-192, doi:10.1146/annurev-biochem-061516-044916.
27. Chahwan, R.; Gravel, S.; Matsusaka, T.; Jackson, S.P. Dma/RNF8 proteins are evolutionarily conserved E3 ubiquitin ligases that target septins. *Cell Cycle* **2013**, *12*, 1000-1008, doi:10.4161/cc.23947.
28. Isakson, P.; Lystad, A.H.; Breen, K.; Koster, G.; Stenmark, H.; Simonsen, A. TRAF6 mediates ubiquitination of KIF23/MKLP1 and is required for midbody ring degradation by selective autophagy. *Autophagy* **2013**, *9*, 1955-1964, doi:10.4161/auto.26085.
29. Wickström, S.A.; Masoumi, K.C.; Khochbin, S.; Fässler, R.; Massoumi, R. CYLD negatively regulates cell-cycle progression by inactivating HDAC6 and increasing the levels of acetylated tubulin. *Embo j* **2010**, *29*, 131-144, doi:10.1038/emboj.2009.317.
30. Magliozzi, R.; Carrero, Z.I.; Low, T.Y.; Yuniati, L.; Valdes-Quezada, C.; Kruiswijk, F.; van Wijk, K.; Heck, A.J.R.; Jackson, C.L.; Guardavaccaro, D. Inheritance of the Golgi Apparatus and Cytokinesis Are Controlled by Degradation of GBF1. *Cell Rep* **2018**, *23*, 3381-3391 e3384, doi:10.1016/j.celrep.2018.05.031.
31. Zanchetta, M.E.; Meroni, G. Emerging Roles of the TRIM E3 Ubiquitin Ligases MID1 and MID2 in Cytokinesis. *Front Physiol* **2019**, *10*, 274, doi:10.3389/fphys.2019.00274.
32. Georges, A.; Coyaud, E.; Marcon, E.; Greenblatt, J.; Raught, B.; Frappier, L. USP7 Regulates Cytokinesis through FBXO38 and KIF20B. *Sci Rep* **2019**, *9*, 2724, doi:10.1038/s41598-019-39368-y.
33. Go, C.D.; Knight, J.D.R.; Rajasekharan, A.; Rathod, B.; Hesketh, G.G.; Abe, K.T.; Youn, J.-Y.; Samavarchi-Tehrani, P.; Zhang, H.; Zhu, L.Y.; et al. A proximity biotinylation map of a human cell. *BioRxiv* **2019**, doi:10.1101/796391.
34. Karess, R.E.; Chang, X.J.; Edwards, K.A.; Kulkarni, S.; Aguilera, I.; Kiehart, D.P. The regulatory light chain of nonmuscle myosin is encoded by spaghetti-squash, a gene required for cytokinesis in Drosophila. *Cell* **1991**, *65*, 1177-1189, doi:10.1016/0092-8674(91)90013-o.
35. Janisch, K.M.; Vock, V.M.; Fleming, M.S.; Shrestha, A.; Grimsley-Myers, C.M.; Rasoul, B.A.; Neale, S.A.; Cupp, T.D.; Kinchen, J.M.; Liem, K.F., Jr.; et al. The vertebrate-specific Kinesin-6, Kif20b, is required for normal cytokinesis of polarized cortical stem cells and cerebral cortex size. *Development* **2013**, *140*, 4672-4682, doi:10.1242/dev.093286.
36. Gregory, S.L.; Shandala, T.; O'Keefe, L.; Jones, L.; Murray, M.J.; Saint, R. A Drosophila overexpression screen for modifiers of Rho signalling in cytokinesis. *Fly (Austin)* **2007**, *1*, 13-22, doi:10.4161/fly.3806.

37. Liu, Y.; Ge, Q.; Chan, B.; Liu, H.; Singh, S.R.; Manley, J.; Lee, J.; Weideman, A.M.; Hou, G.; Hou, S.X. Whole-animal genome-wide RNAi screen identifies networks regulating male germline stem cells in Drosophila. *Nat Commun* **2016**, *7*, 12149, doi:10.1038/ncomms12149.
38. Echard, A.; Hickson, G.R.; Foley, E.; O'Farrell, P.H. Terminal cytokinesis events uncovered after an RNAi screen. *Curr Biol* **2004**, *14*, 1685-1693, doi:10.1016/j.cub.2004.08.063.
39. Somma, M.P.; Fasulo, B.; Cenci, G.; Cundari, E.; Gatti, M. Molecular dissection of cytokinesis by RNA interference in Drosophila cultured cells. *Mol Biol Cell* **2002**, *13*, 2448-2460, doi:10.1091/mbc.01-12-0589.
40. Eggert, U.S.; Kiger, A.A.; Richter, C.; Perlman, Z.E.; Perrimon, N.; Mitchison, T.J.; Field, C.M. Parallel chemical genetic and genome-wide RNAi screens identify cytokinesis inhibitors and targets. *PLoS Biol* **2004**, *2*, e379, doi:10.1371/journal.pbio.0020379.
41. Pollard, T.D. Functional genomics of cell morphology using RNA interference: pick your style, broad or deep. *J Biol* **2003**, *2*, 25, doi:10.1186/1475-4924-2-25.
42. Kiger, A.A.; Baum, B.; Jones, S.; Jones, M.R.; Coulson, A.; Echeverri, C.; Perrimon, N. A functional genomic analysis of cell morphology using RNA interference. *J Biol* **2003**, *2*, 27, doi:10.1186/1475-4924-2-27.
43. Björklund, M.; Taipale, M.; Varjosalo, M.; Saharinen, J.; Lahdenperä, J.; Taipale, J. Identification of pathways regulating cell size and cell-cycle progression by RNAi. *Nature* **2006**, *439*, 1009-1013, doi:10.1038/nature04469.
44. Neggers, J.E.; Paolella, B.R.; Asfaw, A.; Rothberg, M.V.; Skipper, T.A.; Yang, A.; Kalekar, R.L.; Krill-Burger, J.M.; Dharia, N.V.; Kugener, G.; et al. Synthetic Lethal Interaction between the ESCRT Paralog Enzymes VPS4A and VPS4B in Cancers Harboring Loss of Chromosome 18q or 16q. *Cell Rep* **2020**, *33*, 108493, doi:10.1016/j.celrep.2020.108493.
45. Tedeschi, A.; Almagro, J.; Renshaw, M.J.; Messal, H.A.; Behrens, A.; Petronczki, M. Cep55 promotes cytokinesis of neural progenitors but is dispensable for most mammalian cell divisions. *Nat Commun* **2020**, *11*, 1746, doi:10.1038/s41467-020-15359-w.
46. Morita, E.; Sandrin, V.; Chung, H.Y.; Morham, S.G.; Gygi, S.P.; Rodesch, C.K.; Sundquist, W.I. Human ESCRT and ALIX proteins interact with proteins of the midbody and function in cytokinesis. *Embo j* **2007**, *26*, 4215-4227, doi:10.1038/sj.emboj.7601850.
47. Iwamori, T.; Iwamori, N.; Ma, L.; Edson, M.A.; Greenbaum, M.P.; Matzuk, M.M. TEX14 interacts with CEP55 to block cell abscission. *Mol Cell Biol* **2010**, *30*, 2280-2292, doi:10.1128/mcb.01392-09.
48. Christ, L.; Wenzel, E.M.; Liestøl, K.; Raiborg, C.; Campsteijn, C.; Stenmark, H. ALIX and ESCRT-I/II function as parallel ESCRT-III recruiters in cytokinetic abscission. *J Cell Biol* **2016**, *212*, 499-513, doi:10.1083/jcb.201507009.
49. Andersen, C.L.; Jensen, J.L.; Ørntoft, T.F. Normalization of real-time quantitative reverse transcription-PCR data: a model-based variance estimation approach to identify genes suited for normalization, applied to bladder and colon cancer data sets. *Cancer Res* **2004**, *64*, 5245-5250, doi:10.1158/0008-5472.Can-04-0496.
50. Pfaffl, M.W. A new mathematical model for relative quantification in real-time RT-PCR. *Nucleic Acids Res* **2001**, *29*, e45, doi:10.1093/nar/29.9.e45.
51. de Chaumont, F.; Dallongeville, S.; Chenouard, N.; Hervé, N.; Pop, S.; Provoost, T.; Meas-Yedid, V.; Pankajakshan, P.; Lecomte, T.; Le Montagner, Y.; et al. Icy: an open bioimage informatics platform for extended reproducible research. *Nat Methods* **2012**, *9*, 690-696, doi:10.1038/nmeth.2075.
52. Dufour, A.C.; Meas-Yedid, V.; Grassart, A.; Olivo-Marin, J.-C. Automated quantification of cell endocytosis using active contours and wavelets. *2008 19th International Conference on Pattern Recognition* **2008**, 1-4.
53. Manich, M.; Boquet-Pujadas, A.; Dallongeville, S.; Guillen, N.; Olivo-Marin, J.-C. A Protocol to Quantify Cellular Morphodynamics: From Cell Labelling to Automatic Image Analysis. In Proceedings of the Eukaryome Impact on Human Intestine Homeostasis and Mucosal Immunology, Cham, 2020//, 2020; pp. 351-367.

54. Goliand, I.; Nachmias, D.; Gershony, O.; Elia, N. Inhibition of ESCRT-II-CHMP6 interactions impedes cytokinetic abscission and leads to cell death. *Mol Biol Cell* **2014**, *25*, 3740-3748, doi:10.1091/mbc.E14-08-1317.
55. Konstantinidis, D.G.; Giger, K.M.; Risinger, M.; Pushkaran, S.; Zhou, P.; Dexheimer, P.; Yerneni, S.; Andreassen, P.; Klingmüller, U.; Palis, J.; et al. Cytokinesis failure in RhoA-deficient mouse erythroblasts involves actomyosin and midbody dysregulation and triggers p53 activation. *Blood* **2015**, *126*, 1473-1482, doi:10.1182/blood-2014-12-616169.
56. Weinmaster, G.; Fischer, J.A. Notch ligand ubiquitylation: what is it good for? *Dev Cell* **2011**, *21*, 134-144, doi:10.1016/j.devcel.2011.06.006.
57. Koutelou, E.; Sato, S.; Tomomori-Sato, C.; Florens, L.; Swanson, S.K.; Washburn, M.P.; Kokkinaki, M.; Conaway, R.C.; Conaway, J.W.; Moschonas, N.K. Neuralized-like 1 (Neurl1) targeted to the plasma membrane by N-myristoylation regulates the Notch ligand Jagged1. *J Biol Chem* **2008**, *283*, 3846-3853, doi:10.1074/jbc.M706974200.
58. Nayak, D.; Sivaraman, J. Structural basis for the indispensable role of a unique zinc finger motif in LNX2 ubiquitination. *Oncotarget* **2015**, *6*, 34342-34357, doi:10.18632/oncotarget.5326.
59. Hong, J.; Won, M.; Ro, H. The Molecular and Pathophysiological Functions of Members of the LNX/PDZRN E3 Ubiquitin Ligase Family. *Molecules* **2020**, *25*, doi:10.3390/molecules25245938.
60. Sunchu, B.; Cabernard, C. Principles and mechanisms of asymmetric cell division. *Development* **2020**, *147*, doi:10.1242/dev.167650.
61. Trylinski, M.; Schweisguth, F. Activation of Arp2/3 by WASp Is Essential for the Endocytosis of Delta Only during Cytokinesis in Drosophila. *Cell Rep* **2019**, *28*, 1-10.e13, doi:10.1016/j.celrep.2019.06.012.
62. Liu, S.; Boulianne, G.L. The NHR domains of Neuralized and related proteins: Beyond Notch signalling. *Cell Signal* **2017**, *29*, 62-68, doi:10.1016/j.cellsig.2016.10.004.
63. Young, P.W. LNX1/LNX2 proteins: functions in neuronal signalling and beyond. *Neuronal Signal* **2018**, *2*, Ns20170191, doi:10.1042/ns20170191.
64. Flynn, M.; Saha, O.; Young, P. Molecular evolution of the LNX gene family. *BMC Evol Biol* **2011**, *11*, 235, doi:10.1186/1471-2148-11-235.
65. Lynn, B.D.; Li, X.; Hormuzdi, S.G.; Griffiths, E.K.; McGlade, C.J.; Nagy, J.I. E3 ubiquitin ligases LNX1 and LNX2 localize at neuronal gap junctions formed by connexin36 in rodent brain and molecularly interact with connexin36. *Eur J Neurosci* **2018**, *48*, 3062-3081, doi:10.1111/ejn.14198.
66. Lenihan, J.A.; Saha, O.; Young, P.W. Proteomic analysis reveals novel ligands and substrates for LNX1 E3 ubiquitin ligase. *PLoS One* **2017**, *12*, e0187352, doi:10.1371/journal.pone.0187352.
67. Gruneberg, U.; Neef, R.; Li, X.; Chan, E.H.; Chalamalasetty, R.B.; Nigg, E.A.; Barr, F.A. KIF14 and citron kinase act together to promote efficient cytokinesis. *J Cell Biol* **2006**, *172*, 363-372, doi:10.1083/jcb.200511061.
68. Chen, R.H.; Chen, Y.H.; Huang, T.Y. Ubiquitin-mediated regulation of autophagy. *J Biomed Sci* **2019**, *26*, 80, doi:10.1186/s12929-019-0569-y.
69. Yan, C.; Huo, H.; Yang, C.; Zhang, T.; Chu, Y.; Liu, Y. Ubiquitin C-Terminal Hydrolase L1 regulates autophagy by inhibiting autophagosome formation through its deubiquitinating enzyme activity. *Biochem Biophys Res Commun* **2018**, *497*, 726-733, doi:10.1016/j.bbrc.2018.02.140.
70. Matz, A.; Lee, S.J.; Schwedhelm-Domeyer, N.; Zanini, D.; Holubowska, A.; Kannan, M.; Farnworth, M.; Jahn, O.; Göpfert, M.C.; Stegmüller, J. Regulation of neuronal survival and morphology by the E3 ubiquitin ligase RNF157. *Cell Death Differ* **2015**, *22*, 626-642, doi:10.1038/cdd.2014.163.
71. Dogan, T.; Gnad, F.; Chan, J.; Phu, L.; Young, A.; Chen, M.J.; Doll, S.; Stokes, M.P.; Belvin, M.; Friedman, L.S.; et al. Role of the E3 ubiquitin ligase RNF157 as a novel downstream effector linking PI3K and MAPK signaling pathways to the cell cycle. *J Biol Chem* **2017**, *292*, 14311-14324, doi:10.1074/jbc.M117.792754.

72. Jeffery, J.; Neyt, C.; Moore, W.; Paterson, S.; Bower, N.I.; Chenevix-Trench, G.; Verkade, H.; Hogan, B.M.; Khanna, K.K. Cep55 regulates embryonic growth and development by promoting Akt stability in zebrafish. *Faseb j* **2015**, *29*, 1999-2009, doi:10.1096/fj.14-265090.

73. Frosk, P.; Arts, H.H.; Philippe, J.; Gunn, C.S.; Brown, E.L.; Chodirker, B.; Simard, L.; Majewski, J.; Fahiminiya, S.; Russell, C.; et al. A truncating mutation in CEP55 is the likely cause of MARCH, a novel syndrome affecting neuronal mitosis. *J Med Genet* **2017**, doi:10.1136/jmedgenet-2016-104296.